Mon. Not. R. Astron. Soc. **367,** 851–859 (2006) doi:10.1111/j.1365-2966.2006.10019.x

# Polarization of synchrotron radiation from conical shock waves

T. V. Cawthorne★
*University of Central Lancashire, Preston, Lancashire PR1 2HE*

Accepted 2005 December 16. Received 2005 December 9; in original form 2005 October 27

**ABSTRACT**

Simulated images of synchrotron intensity and polarization are presented for a simple, semi-dynamical model of conical shock waves in an astrophysical jet. Earlier work is extended by inclusion of a component of upstream magnetic field parallel to the jet in addition to the tangled (or disordered) component considered in the earlier paper. Results for several cases representing shocks of moderate strength are shown. It is found that the on-axis polarization reflects the upstream magnetic field structure. Off-axis, the electric field of polarization is oblique to the axis and covers a range depending on the shock cone angle and viewing angle. The results are compared with the structure of a bright knot about 0.8 arcsec from the nucleus in the quasar 3C 380, which may be an example of this kind of structure.

**Key words:** galaxies: active – galaxies: jets.

## 1 INTRODUCTION

Among many effects that determine the structure and polarization of radio emission from astrophysical jets, shocks are thought to play a prominent role. They are likely to occur in supersonic flows in which the injection speed varies or which are surrounded by a medium of variable pressure. In either case, if the changes occur on time-scales less than the sound crossing time of the jet then shocks can result. In synchrotron sources where magnetic field is thought to be frozen into the underlying plasma, shocks can change the magnetic field structure and therefore modify the (linear) polarization. This suggests the possibility of using the polarization to study the physical processes occurring in the jet as it propagates outward from the core. The effects of plane shocks normal to the jet axis have been widely examined. If the jet contains an initially tangled field, these tend to produce polarization with electric field perpendicular to the shock front and hence parallel to the jet direction (Laing 1980; Hughes, Aller & Aller 1985; Cawthorne & Wardle 1988). If the jet contains a magnetic field predominantly parallel to the jet then the shock will enhance the transverse component of any ripples in the field and so the degree of polarization will be reduced. The polarization electric vectors remain transverse to the jet direction as long as the energy density of the enhanced ripples in magnetic field remains smaller than that of the parallel field component.

Numerical simulation of jets suggests that conical shock waves with cone axis coincident with the jet axis result when jets become rapidly out of pressure balance with their surroundings (e.g. Bowman, Leahy & Komissarov 1996). In an earlier paper, Cawthorne & Cobb (1990) investigated the effects of plane-oblique shock waves and conical shock waves on jets with an initially tangled magnetic field. A conical shock wave was regarded as the surface formed from a sheaf of plane-oblique shock waves all with the the same inclination to the jet axis. Formulae for the polarization angle and fraction were derived for plane-oblique shock waves and these properties were integrated numerically to give the corresponding results for conical shocks. The wide variation of polarization angle across shock structure was illustrated. It was shown that an integrated polarization with transverse electric field (i.e., mimicking a magnetic field parallel to the jet) could result from the action of conical shocks on a tangled field, but the largest polarization resulting would be no greater than $\simeq$10 per cent. Since polarizations with transverse electric field exceeding this level are often seen in quasar jets, this led to the conclusion that the transverse *E*-field polarization seen in quasars are unlikely to result from the action of shock waves on an underlying tangled field structure. Hence the ordering of magnetic fields in quasars and BL Lac objects, which have mutually orthogonal field structures (Gabuzda et al. 1992; Cawthorne et al. 1993), must arise from fundamentally different processes.

Subsequently, Lister, Marscher & Gear (1998) investigated the possible role of oblique shocks in producing the misalignments between polarization and jet direction in a sample of radio jets. They concluded that the polarization offsets could not be fitted by a single population of oblique shocks with arbitrary inclinations to the jet axis.

Two developments motivated this extension of the earlier work by Cawthorne & Cobb (1990) on polarization of synchrotron radiation from conical shocks. First, the suggestion that stationary components in the parsec-scale jets could be identified with recollimation shocks (e.g. Agudo et al. 2001) has led observers to search for characteristics with which such features could be identified. Second, the improved facilities for VLBI at high frequencies are beginning to enable resolution of transverse structures, which can then be compared to predictions of theoretical models. This paper adopts the simple model used by Cawthorne & Cobb (1990) for emission from plasma excited by a conical shock wave, and extends it in two ways.

★E-mail: tvcawthorne@uclan.ac.uk

First, the polarization is computed for an upstream magnetic field that has both parallel and tangled (or disordered) components, and second, the results are used to compute total intensity and polarization images which are then convolved for comparison with radio images.

At this point it is worth mentioning the origin of the parallel field component. Since flux-conservation requires that any parallel field decays more rapidly than transverse field, it is possible that such field originates in a boundary layer (of unknown width) and some authors (e.g. Laing 1995) have adopted this as a working hypothesis. The intention of the present work is only to illustrate the consequences of conical shocks for some simple cases and from hereon the parallel component of field is assumed to fill the entire jet. However, a useful feature of the model is that it is trivial to adapt to cases such as the boundary layer field, and it is hoped that observers will treat the model as a flexible tool for use in explaining their images.

Section 2 describes the model used in this paper. Section 3 presents a derivation of formulae for the total intensity and polarization in the case where the upstream magnetic field is parallel to the jet. Section 4 summarizes the corresponding results from Cawthorne & Cobb (1990) for the case where the upstream magnetic field is tangled on scales much smaller than the emitting region. Section 5 presents the resulting images for a representative range of models. The type of features that result depend strongly on the angle between the cone axis and the line of sight. Section 6 makes a tentative comparison between the computed images and the structure of a radio knot in the quasar 3C 380. Although the models are probably too simple for a quantitative comparison, the results nonetheless make some clear qualitative predictions of the types of structures likely to be observed in components excited by conical shocks.

## 2 THE MODEL

The model for conical shocks is that suggested by Lind & Blandford (1985) and used later by Cawthorne & Cobb (1990). The model is 'semidynamical' in that it uses the jump conditions to determine the properties of the downstream flow, but ignores subsequent evolution of the flow. The following assumptions are required to avoid a numerical approach.

(i) The conical shock is regarded as a stationary surface formed by a sheaf of plane oblique shocks all making the same angle $\eta$ to the upstream flow.

(ii) The equation of state is assumed to be that of a relativistic gas with specific heat capacity ratio equal to 4/3, and the magnetic field is assumed to be unimportant dynamically. These assumptions simplify the jump conditions dramatically, though the first requires that both electron and proton populations be highly relativistic, or that the plasma consists of electrons and positrons. Little is known about the positively charged particles in jets. Such evidence as there is tends to support the presence of positrons (e.g. Wardle et al. 1998). If protons are present then little is known about their energies and therefore about the heat capacity ratio. In any case it is hard to develop an analytical model without this assumption, which is also retained by many numerical jet simulations.

(iii) The emissivity is greatest while the plasma is still close to the shock front and the emission therefore emerges from a thin layer of material just downstream from the shock. This avoids the need to integrate radiation transfer equations and to follow the dynamic evolution of the downstream flow. The thickness of the emitting layer is assumed independent of frequency, a reasonable assumption if the losses are predominantly due to expansion (though not if the losses are due to radiation).

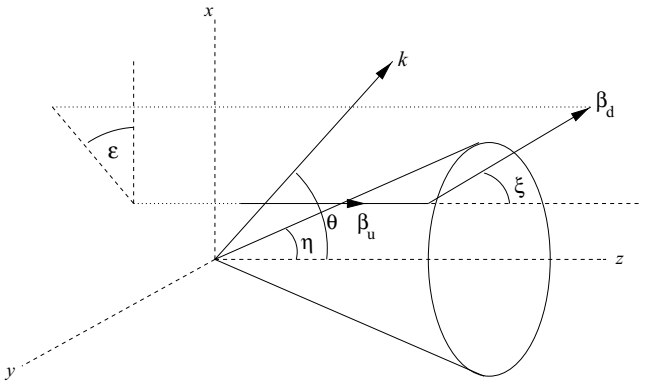


**Figure 1.** This figure illustrates the conical shock model. The conical surface of discontinuity has axis parallel to the $z$-axis and half-opening angle $\eta$. The initial flow velocity $\beta_u$ is parallel to the cone axis, but is deflected through angle $\xi$ to $\beta_d$, which has a projection onto the $x$, $y$ plane making angle $\epsilon$ to the $x$-axis. The structure is viewed by observing wave $k$ in the $x$, $z$ plane which makes angle $\theta$ to the $z$-axis.

(iv) The entire structure remains constant over at least one light-crossing time so that emission may be transformed straightforwardly from one frame to another.

(v) The emitting material is assumed to be optically thin at all rest-frame frequencies corresponding to the frequency of observation.

(vi) On passing through the shock, the synchrotron emitting gas is compressed and its emissivity enhanced. Any component of emission from the upstream plasma is assumed to be negligible by comparison.

The model is illustrated in Fig. 1. The shock is inclined at an angle $\eta$ to the upstream flow velocity, $\beta_u$, and the downstream flow velocity, $\beta_d$, is deflected through an angle $\xi$ towards the shock front. The ray carrying radiation to the observer is parallel to a unit vector labelled $\boldsymbol{k}$ and is inclined at angle $\theta$ to the upstream flow. The $z$-axis is parallel to $\beta_u$ and the $y$-axis is parallel to the vector $\boldsymbol{\beta_u} \times \boldsymbol{k}$. A particular segment of the shock front is denoted by the angle $\epsilon$ between the projection of $\beta_d$ onto the $x$, $y$ plane and the $x$-axis, measured in the sense from $x$ towards $y$.

In Fig. 1, the cone is shown opening towards the observer. However, the same image would result from a cone opening away from the observer if the sky component of upstream velocity is directed in the opposite sense (see Fig. 2).

The downstream velocity, $\beta_d$, and deflection angle, $\xi$, were given by Lind & Blandford (1985) as

$$\beta_d = \frac{\left[\left(1-\beta_u^2\cos^2\eta\right)^2 + 9\beta_u^4\cos^2\eta\sin^2\eta\right]^{1/2}}{(3\beta_u\sin\eta)} \quad (1)$$

and

$$\tan\xi = \frac{\tan^2\eta\left(3\beta_u^2-1\right)-\left(1-\beta_u^2\right)}{\tan\eta\left(\tan^2\eta+1+2\beta_u^2\right)}. \quad (2)$$

The ratio of upstream to downstream number densities (as measured in the respective rest frames) or compression coefficient $\kappa$ is

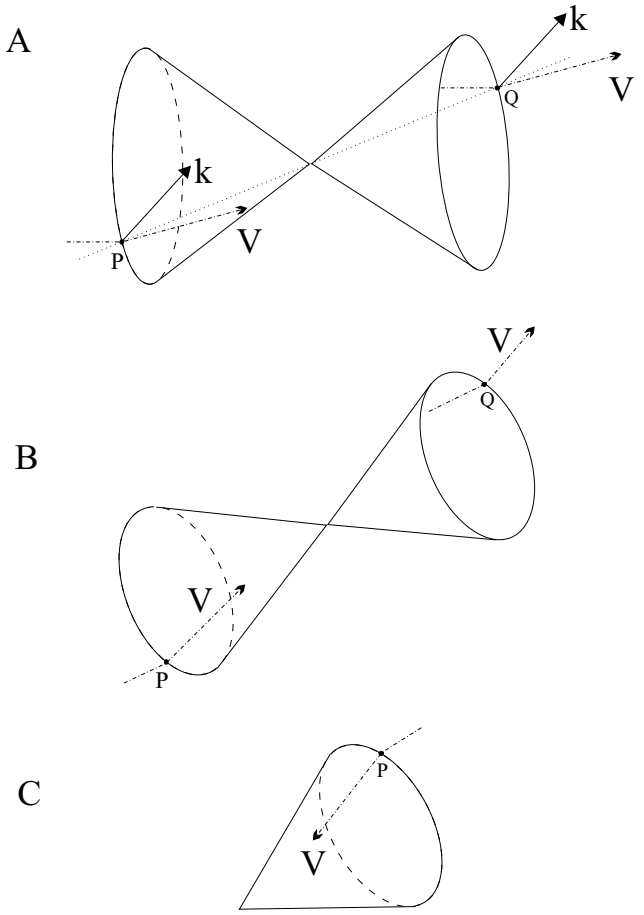


**Figure 2.** This figure demonstrates the equivalence of images resulting from two conical shock surfaces with the same sky projections. One opens towards the observer with upstream velocity directed away from the apex and one opens away from the observer with upstream velocity directed toward the apex. The top figure (A) shows two coaxial cones pointing in opposite directions. Parallel rays $k$ leave the cone at two points P and Q joined by the line parallel through the common apex. Plasma flowing to the right will be deflected by the conical shocks and the resulting velocity vectors $\boldsymbol{V}$ are shown. The orientations of the shock, the velocity vectors and the wave vector are identical at points P and Q, and so the emissive properties (including polarization) will also be identical. The middle figure (B) shows the system as seen along the $\boldsymbol{k}$ vectors. In the lower figure (C) the left-hand cone has been rotated by 180° about $k$, an operation that will not alter the emissive properties (including polarization angle, which has a 180° ambiguity). The intensity and polarization will therefore be identical at Q on the right-hand cone in (B) and at the corresponding point (P) on the rotated cone in (C). Therefore, the model images which follow can be regarded either as cones opening towards or away from the observer, provided the velocities are interpreted correctly. If the sky component of upstream velocity is towards the apex for cones pointing into the hemisphere on the observer's side of the sky plane, the same image results for an equivalent cone reflected in the sky plane for which the sky component of the upstream velocity is directed away from the apex. In both cases, the line of sight upstream velocity components are assumed to be towards the observer.

given by Cawthorne & Cobb (1990):

$$\kappa = \frac{\left(1-\beta_{\rm u}^2\cos^2\eta\right)^{1/2}}{\gamma_{\rm u}\beta_{\rm u}\sin\eta\left(8\beta_{\rm u}^2\sin^2\eta-\gamma_{\rm u}^{-2}\right)^{1/2}}. \quad (3)$$

Throughout the paper primed and double primed symbols refer to quantities measured in the rest frame of the downstream and upstream flows, respectively. An exception is made for magnetic flux density and particle density, which are always the values measured in their respective rest frames.

## 3 EMISSION FROM THE PARALLEL FIELD COMPONENT

In this section, expressions are obtained which enable calculation of the polarization of radiation from the component of shocked fluid which has parallel field upstream.

The polarization angles are straightforward to obtain. The flux-freezing condition requires that in the rest frame of the shock in which the upstream flow is parallel to the cone-axis (i.e., the system shown in Fig. 1) the magnetic flux tubes must remain parallel to the flow in the downstream region, too. Hence in this frame, the electric field of polarization for synchrotron radiation will appear perpendicular to the velocity vectors when viewed from any direction. (This is not so in other frames moving along the symmetry axis, where, in the downstream region, separate segments of the same initial flux tube will be moving along separate but parallel lines rather than the same line. To an observer in any such frame, the electric field of polarization will not in general be perpendicular to the velocity vectors.)

The polarization angle $\chi$ is defined to be measured from $\boldsymbol{\beta_u}\times\boldsymbol{k}$ (i.e., the $y$-axis in Fig. 3) in the sense from $\boldsymbol{\beta_u}\times\boldsymbol{k}$ to the sky projection of the upstream flow velocity (see Fig. 3). The components of downstream velocity in the plane of the sky can easily be found: the component parallel to $\boldsymbol{\beta_u}\times\boldsymbol{k}$ is $\beta_{\rm d}\sin\xi\sin\epsilon$ and the component parallel to the projection of $\boldsymbol{\beta_u}$ is $\beta_{\rm d}(\cos\xi\sin\theta-\sin\xi\cos\epsilon\cos\theta)$. The polarized $E$ field is in the plane of the sky normal to the projection of $\beta_{\rm d}$ and the polarization angle $\chi$, as defined above, can then be found from

$$\tan\chi = \frac{\sin\xi\sin\epsilon}{\sin\xi\cos\epsilon\cos\theta-\cos\xi\sin\theta}. \quad (4)$$

The polarized electric field is perpendicular to the jet on-axis ($\epsilon = 0°, 180°$), as expected. More generally, the electric field is perpendicular to the projection of the velocity vectors which form

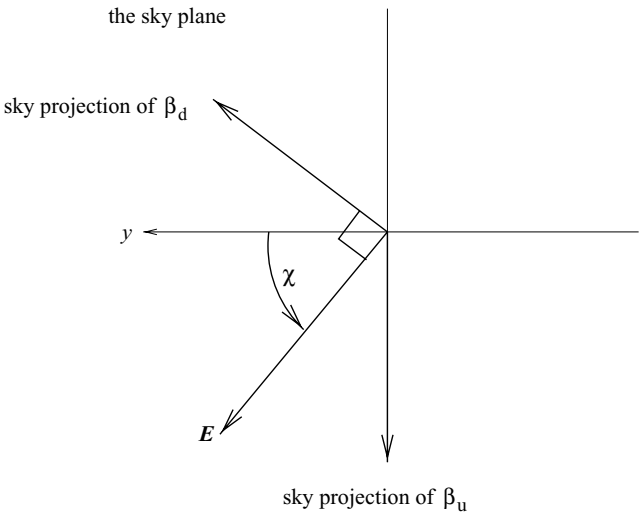


**Figure 3.** This figure shows our definition of the polarization angle $\chi$. The projections of $\beta_{\rm u}$ and $\beta_{\rm d}$ onto the plane of the sky are shown. The electric vector position angle $\chi$ is measured from $\boldsymbol{\beta_u}\times\boldsymbol{k}$ (or the $y$-axis in Fig. 1) in the direction of the projection of $\beta_{\rm u}$.

a cone, apparently diverging from a point on the axis. Viewed from an angle $\theta < \xi$ (or $\theta > 180^\circ - \xi$), the projections of velocity vectors range in direction through a full 360°. The polarization sticks therefore range in direction through a full 180°. However, viewed from an angle $\theta$ in the range $\xi < \theta < 180^\circ - \xi$, the velocity vectors make a maximum angle to the axis where they are tangential to the base of the cone of velocity vectors, at which point $\epsilon = \epsilon_1$ and $\cos\epsilon_1 = \tan\xi/\tan\theta$. Here, the Electric Vector Position Angle (EVPA) is $\chi_1$, where $\tan\chi_1 = -\tan\xi/(\sin\epsilon_1 \sin\theta)$, according to the definition of Fig. 3. The values of $\chi$ therefore range from zero (at $\epsilon = 0$) to $\chi_1$ at $\epsilon_1$ and back to zero at $\epsilon = 180^\circ$.

The fractional polarization for synchrotron radiation from the shocked plasma will be $m_0$, the value for a uniform field; this is normally about 0.7, but depends somewhat on spectral index (e.g. Pacholczyk 1970).

In addition to the number density and upstream magnetic field, which are the same for all parts of the shock surface, the total intensity for the shocked downstream region depends on the Doppler factor $D$ and the angle $\Omega'$ between the line of sight and magnetic field in the rest frame of the emitting gas.

The angle between the downstream flow and $k$ in the shock frame is $\Omega$, where

$$\cos\Omega = \frac{\boldsymbol{k}\cdot\boldsymbol{\beta}_\mathrm{d}}{\beta_\mathrm{d}} = \sin\theta\sin\xi\cos\epsilon + \cos\theta\cos\xi. \quad (5)$$

Since $c\cos\Omega$ is the component of the wave velocity parallel to $\beta_\mathrm{d}$, we may transform this angle into the rest frame of the downstream flow using

$$\cos\Omega' = \frac{\cos\Omega - \beta_\mathrm{d}}{1 - \beta_\mathrm{d}\cos\Omega}. \quad (6)$$

In the rest frame of the downstream gas, the downstream field is parallel to the transformation axis and so $\Omega'$ can also be interpreted as the angle between the magnetic field and line of sight, which (along with the magnetic flux density) determines the emissivity in direction $k$.

The Doppler beaming factor for radiation from the downstream flow is clearly

$$D = \frac{1}{\gamma_\mathrm{d}(1 - \beta_\mathrm{d}\cos\Omega)}, \quad (7)$$

where as usual $\gamma_\mathrm{d} = (1 - \beta_\mathrm{d}^2)^{-1/2}$.

In the rest frame of the upstream plasma the parallel component of magnetic flux density has field strength $B_\mathrm{p}$ and the shock has inclination $\eta''$ where $\tan\eta'' = \gamma_\mathrm{u}\tan\eta$. In the same frame the components of magnetic field parallel and perpendicular to the shock will be $B_{||,\mathrm{u}} = B_\mathrm{p}\cos\eta''$ and $B_{\perp,\mathrm{u}} = B_\mathrm{p}\sin\eta''$, respectively. Downstream from the shock, the component of field normal to the shock is unaltered while the flux-freezing condition requires that the component parallel to the shock is enhanced by a factor $\kappa^{-1}$. Hence the downstream field components are $B_{||,\mathrm{d}} = B_\mathrm{p}\cos\eta''/\kappa$ and $B_{\perp,\mathrm{d}} = B_\mathrm{p}\sin\eta''$. The downstream field will therefore be

$$B_\mathrm{p,d} = B_\mathrm{p}\left(\sin^2\eta'' + \frac{\cos^2\eta''}{\kappa^2}\right)^{1/2} = B_\mathrm{p}\left(\frac{1 + \kappa^2\gamma_\mathrm{u}^2\tan^2\eta)}{\kappa^2\left(1 + \gamma_\mathrm{u}^2\tan^2\eta\right)}\right)^{1/2}. \quad (8)$$

The emission is from a thin, conical layer downstream from the shock, with thickness independent of distance from the axis. The intensity to emerge from a path-length $l$ through the emitting layer is given in terms of the emission coefficient for the parallel-field component of the downstream gas $j_{\nu,\mathrm{p}}$ by

$$I = j_{\nu,\mathrm{p}}\, l = j'_{\nu,\mathrm{p}} D^{2+\alpha} l, \quad (9)$$

where $j'_{\nu,\mathrm{p}}$ is the emission coefficient in the rest frame of the downstream gas (e.g. Rybicki & Lightman 1979), where $D$ is not constant but varies across the shock. The rest-frame emission coefficient is the standard result for synchrotron radiation from a plasma with a uniform magnetic field

$$j'_{\nu,\mathrm{p}} = C n_\mathrm{d}(B_\mathrm{p,d}\sin\Omega')^{1+\alpha}\nu^{-\alpha}, \quad (10)$$

where $\alpha$ is the optically thin spectral index, $n_\mathrm{d}$ is the density of relativistic electrons in the downstream region and $C$ depends only on $\alpha$ (weakly) and fundamental constants (e.g. Pacholczyk 1970).

## 4 EMISSION FROM THE TANGLED FIELD COMPONENT

Synchrotron emission from the shocked-tangled field component was described by Cawthorne & Cobb (1990). The notation in that paper is the same as that used here except that the orientation of $\beta_\mathrm{d}$ was specified by angle $\phi$ in Cawthorne & Cobb (1990) where $\epsilon = -\phi$; the polarization angle used in that paper is referred to here as $\chi_\mathrm{cc}$ and is related to the polarization angle used here by $\chi_\mathrm{t} = 180^\circ - \chi_\mathrm{cc}$. Hence from Cawthorne & Cobb (1990)

$$\tan\chi_\mathrm{t} = \frac{\cos\epsilon\cos\eta(\beta_\mathrm{u} - \cos\theta) - \sin\eta\sin\theta}{\sin\epsilon\cos\eta(1 - \beta_\mathrm{u}\cos\theta)}. \quad (11)$$

As discussed in Cawthorne & Cobb (1990), the polarization angles are most easily understood in the rest frame of the upstream flow where the electric field of the polarized wave is parallel to the projected downstream velocity vector. Hence at $\epsilon = 0^\circ$ and 180° the polarized electric field is parallel to the projected axis. In this frame, velocity vectors make an angle $90^\circ + \eta''$ to the $z''$-axis and form a cone diverging from a point on the axis. If viewed from $\theta'' < 90^\circ - \eta''$ (or from $\theta'' > 90^\circ + \eta''$), the projected direction of the velocity vectors onto the sky plane ranges through a full 360° and so $\chi$ ranges through a full 180°. However, if viewed from $\theta''$ in the range $90^\circ + \eta'' > \theta'' > 90^\circ - \eta''_\mathrm{u}$, the velocity makes a maximum angle to the projected axis at $\cos\epsilon_2 = -1/(\tan\eta''\tan\theta'')$ where, in the rest frame of the upstream flow, the projected downstream velocity vectors are tangential to the projected base of the cone formed by all downstream velocity vectors. At this point $\chi$ reaches its extreme value given by $\tan\chi_2 = -(\cos\epsilon_2\cos\theta'' + \tan\eta''\sin\theta'')/\sin\epsilon_2$ and the polarized electric field is perpendicular to the projected edge of the conical shock. Hence $\chi$ varies from −90° at $\epsilon = 0$ to a value between −90° and 0° at $\epsilon = \epsilon_2$, giving a range of $\chi$ less than 90° (with $\chi$ as defined in Fig. 3).

The intensity and polarization of emission from the tangled field component depends on the angle $\psi'$ between the normal to the plane of compression and the line of sight in the rest frame of the downstream plasma. This may be found by first resolving the wave vector $\boldsymbol{k}$ into components parallel and perpendicular to the upstream flow and then transforming them into the rest frame of the upstream plasma (denoted by a double prime, as before). From the parallel and perpendicular components $k''_{||}$ and $k''_\perp$, the component normal to the shock front $k''_\mathrm{n}$ may be found and then transformed into the rest frame of the downstream plasma. The parallel component is $k''_{||} = (\cos\theta - \beta_\mathrm{u})/(1 - \beta_\mathrm{u}\cos\theta)$ and the perpendicular component in the $\beta_\mathrm{u}$, $\beta_\mathrm{d}$ plane is $k''_\perp = \sin\theta\cos\epsilon/(\gamma_\mathrm{u}[1 - \beta_\mathrm{u}\cos\theta])$. The component $k''_\mathrm{n}$ normal to the shock front is equal to $k''_{||}\sin\eta'' - k''_\perp\cos\eta''$, $\tan\eta'' = \gamma_\mathrm{u}\tan\eta$. The component of $k''$ normal to the shock

front (which is also normal to the downstream flow in this frame) can then be found by transforming $k''_{\rm n}$ using the velocity $\beta''_{\rm d} = 3\beta_{\rm u} \sin\eta''/2 - 1/(2\beta_{\rm u}\sin\eta'')$. Thus

$$\cos\psi' = \frac{k''_{\rm n} + \beta''_{\rm d}}{1 + k''_{\rm n}\beta''_{\rm d}}. \tag{12}$$

The total intensity for emission from the tangled field component will be

$$I_{\rm t} = j_{\nu,{\rm t}}\, l = j'_{\nu,{\rm t}} D^{2+\alpha} l. \tag{13}$$

The emission coefficient for the tangled field component is obtained from equation (A10) in Hughes et al. (1985) as

$$j'_{\nu,{\rm t}} = C n_{\rm d} \frac{B_{\rm t}^2}{3\kappa^2}(2 - \sin^2\psi'\,(1-\kappa^2))\nu^{-\alpha}, \tag{14}$$

and the fractional polarization is

$$m_{\rm t} = m_0 \frac{(1-\kappa^2)\sin^2\psi'}{2 - \sin^2\psi'(1-\kappa^2)}. \tag{15}$$

Equations (14) and (15) are correct for $\alpha = 1$. Equation (15) is a good approximation for other reasonable values of $\alpha$.

## 5 COMPUTATION OF EMISSIVITY

Calculations were performed assuming that the emission region consists of a thin conical layer of thickness, electron number density and magnetic field all independent of distance from the axis. To use the simplified formulae for the tangled field emission presented in the last section, the optically thin spectral index is assumed to be $\alpha = 1$. For each calculation, we assume a that a fraction $f$ of the stored magnetic energy is in the uniform field component, and a fraction $(1 - f)$ is in disordered field. For each pixel in the image the contribution from both components is calculated by first solving for the value(s) of $\epsilon$ at each point and then using the results given in Sections 2–4. When the line of sight lies inside the conical surface ($\eta > \theta$) there is just one element of the surface contributing to each pixel. When the line of sight is outside the shock ($\theta > \eta$) then for some pixels, the contributions from both the near and far side of the cone must be included.

The emissivity for each pixel must be multiplied by the path-length $l$ through the emitting layer (assumed uniform). The emitting region can be regarded as that between two coaxial cones separated by a distance $z_0$ along their axis. In the coordinate system of Fig. 1, the observed ray is parallel to the $x$, $z$ plane at a particular value of $y$, $y = y_0$, for each element. The intersection between the cone and the plane $y = y_0$ makes an angle $\mu$ with the $z$-axis where $\tan\mu = \tan\eta/\cos\epsilon$ as shown in Fig. 4. Noting that $\mu$ is negative for $\pi/2 < \epsilon < 3\pi/2$, the path-length through the emitting region used in equations (9) and (13) can be approximated by

$$l = z_0 \left| \frac{\sin\mu}{\sin(\theta - \mu)} \right|. \tag{16}$$

(Note that for some orientations of the cone, the line of sight lies very close to parts of the cone surface. In these orientations the volume weighting factor given by equation (16) becomes very large, leading to sharp spikes in intensity which dominate the entire structure. Such large factors are are not physically reasonable since they do not take into account curvature of the surface, due to which the line of sight remains within the emitting region over a shorter distance than predicted. For this reason results for which such large path-length factors occur are not presented.)

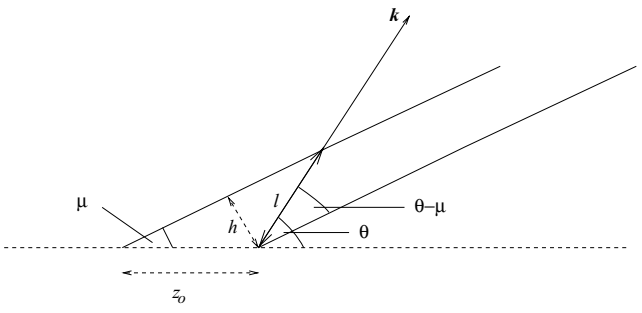


**Figure 4.** A cross-section parallel to the $x$, $z$ plane showing the intersection with (a short section of) two coaxial, conical surfaces. The emitting region is between these surfaces. $l$ is the path-length of the ray $k$ through the emitting region.

## 6 RESULTS

To illustrate the results of these calculations, simulated images from a number of combinations of parameters are shown. Results are shown only for shocks of only modest strength. Since the motivation for this work comes from standing features in astrophysical jets, strong shocks would be of less interest since they deplete a jet's kinetic energy dramatically, preventing further progress downstream. This is in contradiction to observation, where it is seen that standing features in jets do not usually hinder their progress onto larger scales. A cone angle of 20° and an upstream speed $\beta_{\rm u} = 0.95$, or $\gamma_{\rm u} = 3.3$ have therefore been chosen. These give a value for $\kappa \simeq 0.50$ and $\beta_{\rm d} \simeq 0.92$. These results serve to illustrate the most important features resulting from models for shocks of weak to moderate strength given by values of $\beta_{\rm u}$ thought to apply to jets in active galaxies.

For each group of results a row of four plots is shown. The first of these shows a grey-scale 'image' showing the total intensity image predicted by equations (9) and (13). The values of $\theta$ and $\eta$ (in degrees), $f$ and $\beta_{\rm u}$ are given above the plot. The ratio of the flux densities corresponding to black and white in the grey-scale plot is given below.

The second panel shows the variation with distance across the width of the jet of each of the principle terms in the expression for the total intensity, for one value of projected distance $z_{\rm p}$ along the jet (given above the frame). Where the line of sight lies outside the cone, this panel shows variations for either the near or far side of the jet that contributes to the emission, as indicated in the label below the plot. The continuous line represents the variation in intensity due to the change in Doppler shift (proportional to $D^{2+\alpha} = D^3$). The maximum value of $D^3$ is given above the frame. The dashed line represents the variation in the path-length through the emitting layer, $l$, given by equation (16). The dotted line represents the variation in emissivity of the parallel field component due to the variation in viewing angle (in the rest frame of the emitting plasma) as given by equation (10). The dot–dash line represents the variation in emissivity of the tangled field component due to the variation in viewing angle (in the rest frame of the emitting plasma) as given by equation (14). The ratio of the maximum value of the tangled to the parallel field emissivity is given by the ratio $j_{\max{\rm t}}/j_{\max{\rm p}}$ given above the frame. These plots provide an explanation of the causes of variations in brightness across the jet.

The third panel shows the variation in the total polarization with sticks of length proportional to the polarized flux density and orientation given by $\chi$, the $E$-field polarization angle.

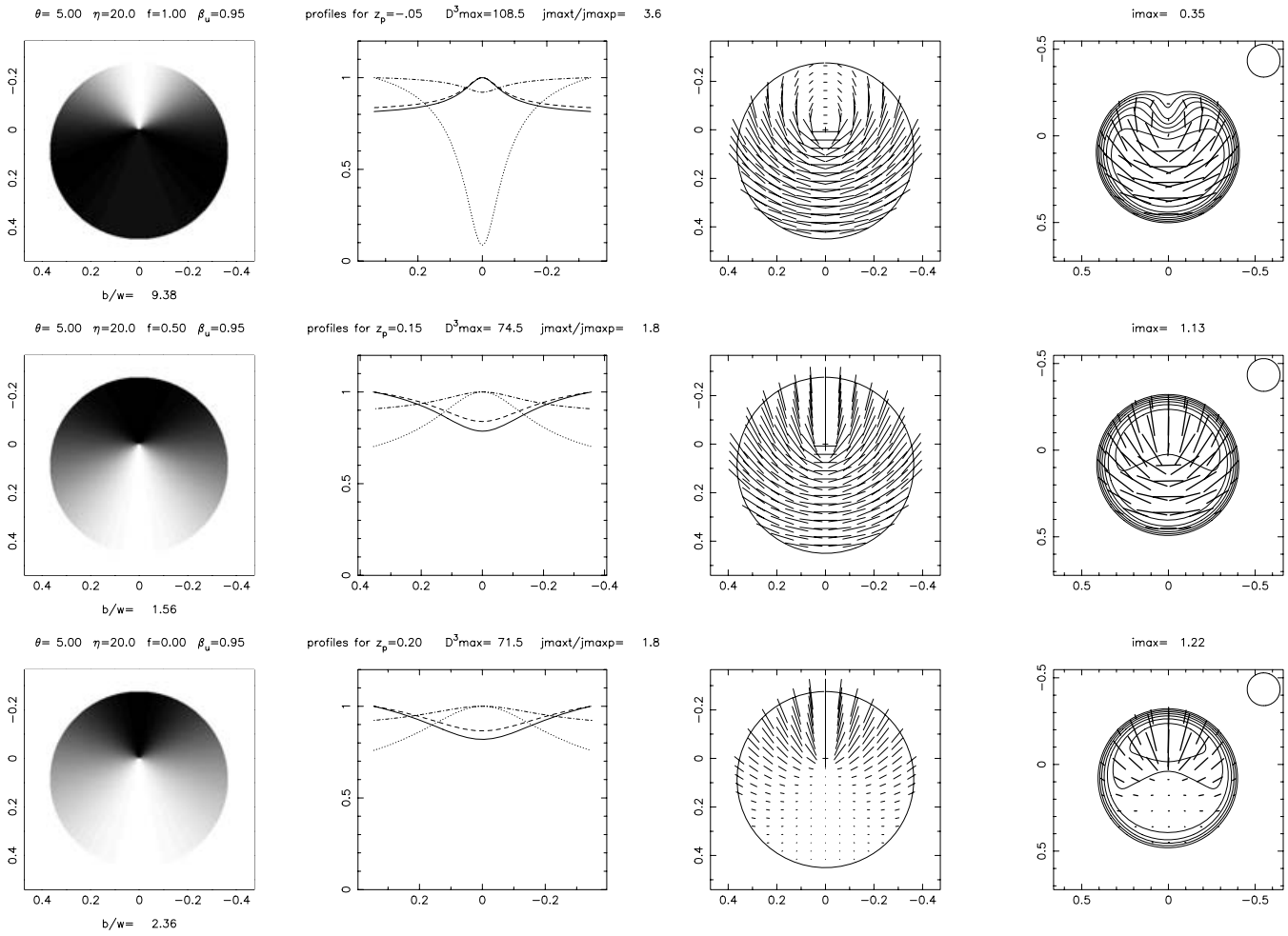


**Figure 5.** Simulated emission from the shocked plasma for $\theta = 5^\circ$ and $\eta = 20^\circ$. The rows correspond to values of $f$ of (from top to bottom) 1.0, 0.5 and 0.0. The plots are described in Section 6.

The fourth panel shows the results of convolution with a beam shown in the top right-hand corner. The total intensity is given by contours which increase by factors of $\sqrt{2}$, beginning at 10 per cent of the peak. The polarization is indicated by sticks, as for the previous panel. The length of a stick of flux density corresponding to the maximum total intensity is given by the value of $i_{\max}$ above the plot. This can be used to determine the fractional polarization.

Each figure shows three such rows, having the same $\eta$ and $\theta$ and $f = 0$, 0.5 and 1.0 in the first, second and third rows, respectively. The curves in the panels showing the variation of emissivity, Doppler boosting and path-length across the width of the jet do not depend on $f$ and so each of those plots in any given figure apply to each row in that figure.

The first group of images (Fig. 5) shows results for a line of sight within the cone of the shock and 5° from the cone axis.

For the parallel field case, the total intensity is strongest at the far side of the cone, with a deep minimum in the centre of the near side. This minimum occurs because at this point, the line of sight is only 1.9° from the velocity in the shock frame and only 9.1° from the velocity in the frame of the downstream flow. This leads to a term $\sin^2 9.1^\circ \simeq 0.025$ in the expression for the emissivity as illustrated by the second plot in this row (dotted line). For the tangled field case, the total intensity is brightest at the near side of the jet and shows a shallow minimum at the centre of the far side, chiefly due to the variations in Doppler shift and path-length (as shown by the second plot).

The polarized intensity follows the same pattern as the total intensity for the parallel field case, since the fractional polarization is constant. In the tangled field case, however, the minimum in polarized intensity at the far side of the jet is much deeper than that in total intensity because the percentage polarization is only about 1 per cent here. This low value is due to the small angle (only about 7°) between the line of sight and the normal to the plane of compression in the frame of the downstream flow.

For the case of $f = 0.5$ (initially equal energies in tangled and parallel field), the polarization of the near side of the jet is dominated by the tangled field component whilst that of the far side of the jet is dominated by the parallel field component. This leads to a sudden 90° change in $\chi$ along the axis.

For $\theta = 5^\circ$, both tangled and parallel field components have values of $\chi$ that rotate through a full 180° as discussed in Sections 3 and 4. For the parallel field case ($f = 1$, top row), this full range of $\chi$ can be seen. However, in the tangled field case ($f = 0$, third row), most of the variation in $\chi$ occurs at the lower part of the cone (near $\epsilon = 180^\circ$) where the polarization is weak and only a limited range of $\chi$ is therefore apparent. For the remaining figures shown here for larger values of $\theta$, the polarization angles have a variation less than 180° in both the parallel field and tangled field cases.

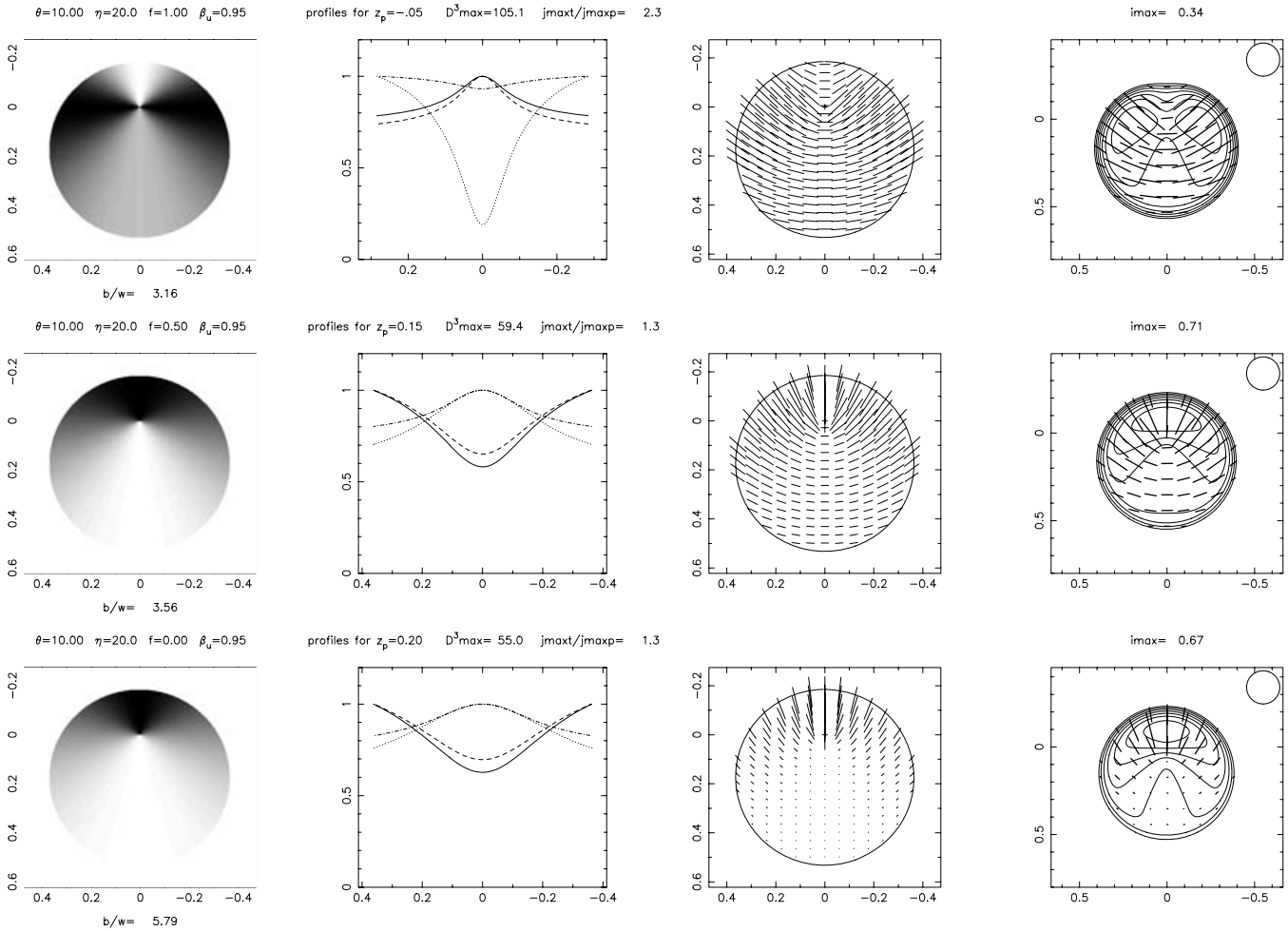


**Figure 6.** Simulated emission from the shocked plasma for $\theta = 10^\circ$ and $\eta = 20^\circ$. The rows correspond to values of $f$ of (from top to bottom) 1.0, 0.5 and 0.0. The plots are described in Section 6.

The second group of images (Fig. 6) shows results for a line of sight inside the cone of the shock 10° from the cone axis. As in the case of $\theta = 5^\circ$, the total intensity is brightest on the near side of the cone for the tangled field ($f = 0$) case. In the parallel field ($f = 1$) case, the total intensity is brightest in the wings either side of the apex, leading to a double-humped intensity structure in the convolved image (fourth plot, top row). In the tangled field case, the percentage polarization is again very low on the far side of the jet (since the line of sight again lies close to the normal to the compression plane in the frame of the downstream flow). For the intermediate case of $f = 0.5$, the polarization is again dominated by the tangled field component on the near side and the parallel field component on the far side, leading to a sudden change in $\chi$ of 90° along the axis, as in the previous figure.

The biggest change from the $\theta = 5^\circ$ case is that the range of polarization angles in the parallel field case ($f = 0$) is now notably less than 180° since the line of sight lies outside the cone formed by the downstream velocity vectors.

Fig. 7 shows results for $\theta = 35^\circ$, a line of sight outside the cone. In this case both the near and far side of the jet contribute to the brightness in some regions, though the near side dominates, due mainly to larger Doppler factors and geometric (path-length) effects (as shown by the second panel in each row). In the parallel field case, the polarization sticks have a limited range of orientation, near perpendicular to the jet axis (since the projected downstream velocities are close to the axis). In the tangled field case, the polarization sticks at the edge of the jet are perpendicular to the edge, as expected, whilst on axis they are parallel to the axis, also as expected.

## 7 APPLICATION OF THE RESULTS

As a result of the sweeping simplifications adopted by this paper, it is probably inappropriate to use the results as the basis for detailed modelling. However, in the case of jet features that are much brighter than their surroundings (as in the case of cores) or well separated from other parts of the jet, the results presented offer an overview of the types of structures that might be generated by conical shock waves. The model is straightforward to encode and it is hoped that investigators will use it as a tool to assist in interpretation of their own data.

One example of such an application is provided by a knot in the jet of the quasar 3C 380. 1.6-GHz Very Long Baseline Array (VLBA) observations revealed the presence of two distinct knots, K1 and K2, at distances of, respectively, 0.75 and 1.1 arcsec from the core. These are clearly seen in the VLA images presented by O'Dea et al. (1999) and also in the VLBA images presented by Kameno et al.

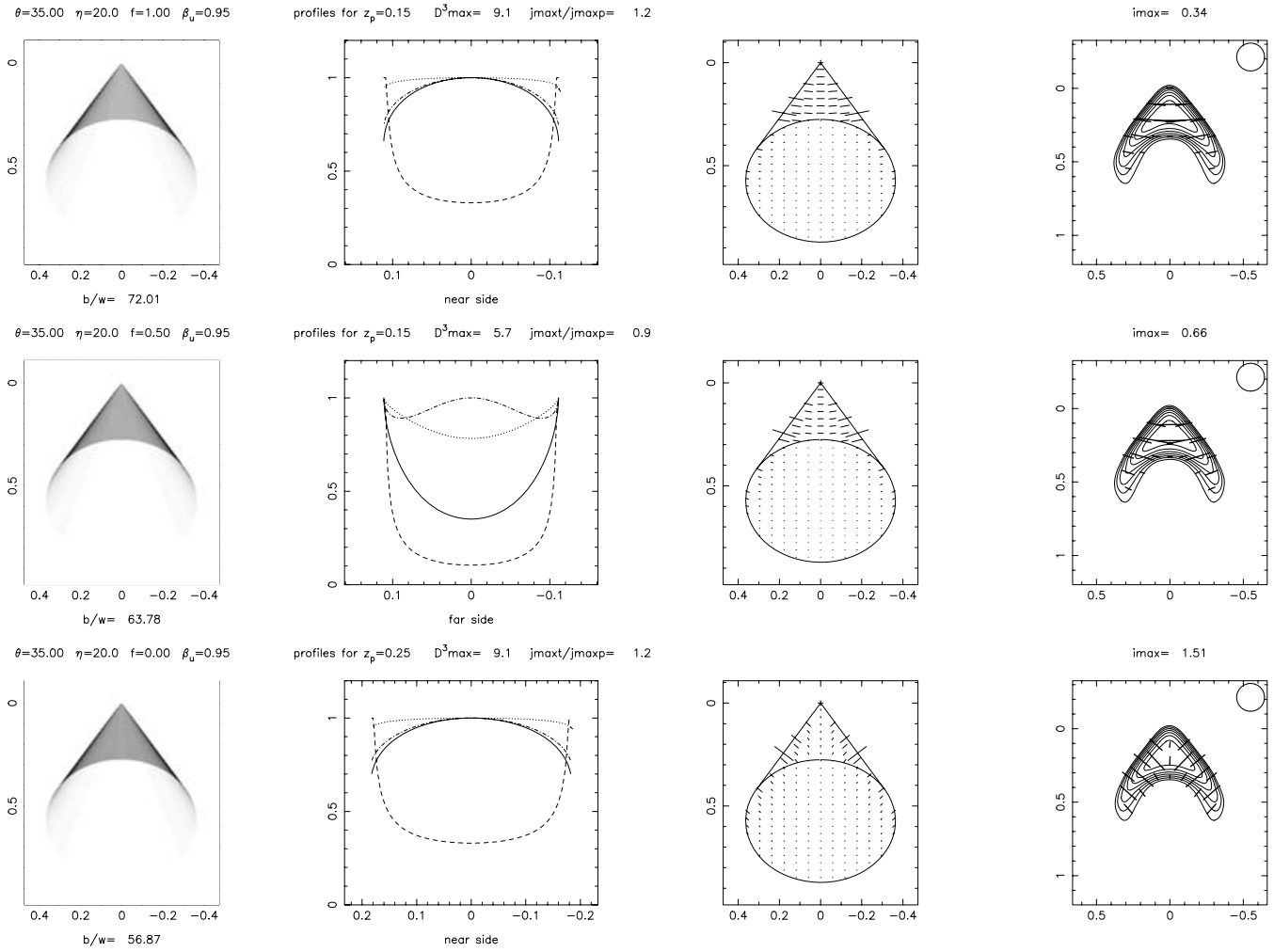


**Figure 7.** Simulated emission from the shocked plasma for $\theta = 35^\circ$ and $\eta = 20^\circ$. The rows correspond to values of $f$ of (from top to bottom) 1.0, 0.5 and 0.0. The plots are described in Section 6.

(2000a,b). [K1 is visible in the top right-hand of Fig. 1(a) of Kameno et al. (2000a), while both knots are visible, though less clearly, in Fig. 1 of Kameno et al. (2000b).] These knots, which, together with the bright nuclear component lie, approximately, on a straight line, both show total intensity structure brightest at the edge facing the nuclear component. Polarization-sensitive observations of the knot K1 (Papageorgiou 2005; Papageorgiou et al., in preparation) show features reminiscent of the conical shock simulations presented in the previous section. The total intensity contour image (made using the inner five VLBA antennas) together with polarized intensity sticks (here showing *magnetic* vector position angles) is shown in Fig. 8. On the bright south-eastern side of the component (the side facing the nuclear component), the B sticks (which have been rotated by $-65^\circ$ in accordance with an estimate of the Faraday rotation at this position) point to within $10^\circ$ of the nuclear component. Further from the nucleus (towards the north-west side of the component), polarization is only detected in patches, but where it is detected, the polarization vectors show signs of a fan pattern, as seen in Figs 4–6. For comparison, the case of $\eta = 20^\circ$, $\theta = 10^\circ$, $\beta = 0.95$ and $f = 0.5$ (from Fig. 5) is reproduced in Fig. 7 (now showing $B$ polarization angles), and rotated for approximate alignment with the image. This is in no sense intended as a fit to the image, but it is worth noting that the model percentage polarization at the $I$ peak is 0.3, very close to the observed level at this position in K1.

It is interesting to note that there is an optical knot at the position of K1 (O'Dea et al. 1999; Kameno et al. 2000a). The short lifetimes of the radiating electrons suggest re-acceleration, as expected in the vicinity of a shock.

The VLBA observations of this region in 3C 380 were not well matched to the angular scales involved, and better matched observations are planned in the near future. In particular, it is hoped to obtain a more complete polarization image, to check for possible ambiguities in the measurement of rotation measure and to obtain more complete coverage of polarized intensity.

Other examples of structures that could be represented by conical shocks include the cores of some radio sources observed at high frequency. This would be consistent with the identification of the core with the first and strongest of a series of standing recollimation shocks, as suggested by Marscher & Daly (1988). For example, the core of 1803+784 observed at 43 GHz by Jorstad et al. (2005) shows fan-like patterns of E-vectors at many epochs, reminiscent of the $f = 0$ case in Fig. 5 (i.e. purely tangled field upstream and a small viewing angle). These similarities will be discussed in more detail in a later paper.

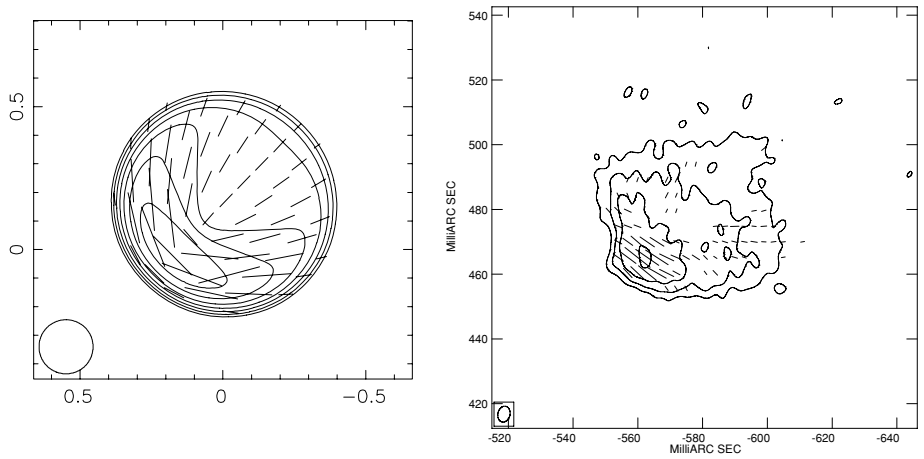


**Figure 8.** Left: Conical shock simulation for $\eta = 20^\circ$, $\theta = 10^\circ$, $\beta_u = 0.95$ and $f = 0.5$, as in Fig. 6, but with *magnetic* field polarization sticks. Right: For comparison, knot K1 in 3C 380 as imaged at 1.6 GHz by the inner five VLBA antennas. Contours represent total intensity at levels $(-1, 1, 2, 4\ldots) \times 2$ mJy beam$^{-1}$. Magnetic field polarization sticks with length proportional to polarized intensity. The peak polarized flux density is 15 mJy beam$^{-1}$.

## 8 CONCLUSIONS

Formulae that allow computation of total intensity and polarization of synchrotron emission from a plasma subject to an oblique shock with upstream magnetic field parallel to the flow direction are presented. These results complement those presented earlier by Cawthorne & Cobb (1990) for a plasma with a disordered (or tangled) upstream field. The results are used to present simulated images of emission from conical shock waves such as may be responsible for emission from stationary features in jets where the upstream magnetic field consists of a uniform parallel component and a disordered component.

These results depend on a number of assumptions, in particular, that the emission emerges from near the shock so that the subsequent evolution of the downstream flow can be ignored. However, they have the merit of being analytically tractable and are easy to compute. As such they allow a useful first step in the comparison between the polarization signatures observed in jets and theoretical models. Results are shown for a few representative cases of shocks of moderate strength.

The overall shape of the simulated image deviates from circularity as the angle between the cone axis and the line of sight increases. This is due to the changing outline of the structure and the increasing ratios of the near-side to far-side Doppler shifts and path-lengths. The on-axis polarization usually reflects the dominant upstream magnetic field structure, with disordered and parallel field yielding EVPA sticks parallel to the axis and perpendicular to the axis, respectively. In cases where both field structures are present, the on-axis $\chi$ reflect the dominant emissivity, which may change along the axis, leading to a $90^\circ$ change in the on-axis values of $\chi$.

The overall range in $\chi$ depends on the viewing angle. A full range of $\chi$ of $180^\circ$ is only seen for $\theta$ less than the deflection angle $\xi$ or greater than $180^\circ - \xi$ in the parallel field case, and for $\theta'' < 90^\circ - \eta''$ or greater than $90^\circ + \eta''$ in the tangled field case.

The total and polarized intensity images of knot K1 in 3C 380 show similarities to one of the simulations presented here, suggesting that it may result from a conical shock wave in the jet.

## ACKNOWLEDGMENTS

This work began during a visit to the Instituto de Astrofisica de Andalucia, Granada, funded by the Royal Society and hosted by Dr J.-L. Gomez, to whom thanks are due for suggestions and advice. The author thanks A. L. Papageorgiou for permission to include his image of the radio knot in 3C 380 and A. M. Stirling, J. F. C. Wardle, A. P. Marscher and the referee for useful comments. Support from the Particle Physics and Astronomy Research Council (PPARC) research grants is acknowledged gratefully. The VLBA is operated by the US National Radio Astronomy Observatory, by agreement with Associated Universities Inc.

## REFERENCES

Agudo I., Gomez J.-L., Marti J.-M., Ibanez J.-M., Marscher A. P., Alberdi A., Aloy M.-A., Hardee P. E., 2001, ApJ, 549, L183
Bowman M., Leahy J. P., Komissarov S. S., 1996, MNRAS, 279, 899
Cawthorne T. V., Cobb W. K., 1990, ApJ, 350, 536
Cawthorne T. V., Wardle J. F. C., 1988, ApJ, 332, 696
Cawthorne T. V., Wardle J. F. C., Roberts D. H., Gabuzda D. C., 1993, ApJ, 416, 519
Gabuzda D. C., Cawthorne T. V., Wardle J. F. C., Roberts D. H., 1992, ApJ, 388, 40
Hughes P. A., Aller H. D., Aller M. F., 1985, ApJ, 298, 301
Jorstad S. G. et al., 2005, AJ, 130, 1418
Kameno S., Inoue M., Fujisawa K., Shen Z.-Q., Wajima K., 2000a, PASJ, 52, 1045
Kameno S., Shen Z.-Q., Inoue M., Fujisawa K., Wajima K., 2000b, in Hirabayashi H., Edwards P. G., Murphy D. W., eds, Astrophysical Phenomena Revealed by Space VLBI. Institute of Space and Astronautical Science, Kanagawa, Japan, p. 63
Laing R., 1980, MNRAS, 193, 427
Laing R., 1995, in Hardee P. E., Bridle A. H., Zensus J. A., eds, ASP Conf. Ser. Vol. 100, Energy Transport in Radio Galaxies and Quasars. Astron. Soc. Pac., San Francisco, p. 241
Lind K. R., Blandford R. D., 1985, ApJ, 295, 358
Lister M. L., Marscher A. P., Gear W. K., 1998, ApJ, 504, 702
Marscher A. M., Daly R. A., 1988, ApJ, 334, 539
O'Dea C., de Vries W., Biretta J., Baum S., 1999, AJ, 117, 1143
Pacholczyk A., 1970, Radio Astrophysics. Freeman & Co., San Fransisco
Papageorgiou A. L., 2005, PhD thesis, Univ. Central Lancashire
Rybicki G. B., Lightman A. P., 1979, Radiative Processes in Astrophysics. Wiley, New York
Wardle J. F. C., Homan D. C., Ojha R., Roberts D. H., 1998, Nat, 395, 457

This paper has been typeset from a TEX/LATEX file prepared by the author.